JOURNAL OF MATERIALS SCIENCE **36** (2001) 4535–4542

Oxide layer development under thermal cycling and its role on damage evolution and spallation in TBC system

M. Y. ALI, X. CHEN, G. M. NEWAZ*
Department of Mechanical Engineering, Wayne State University, Detroit, MI 48202, USA
E-mail: gnewaz@eng.wayne.edu

The nature and cause of failure of thermal barrier coatings (TBCs) consisting of physical vapor deposited (PVD) yttria stabilized zirconia (YSZ, 8 wt.% Y_2O_3) and a diffusion aluminide bond coat (Pt-Al) were investigated after oxidative thermal cycling and isothermal heat treatment at 1177 °C in air. Experiments were conducted for 45 and 10-minute hold times and for isothermal condition for disk specimens with and without TBC. It is found that microcracks starts in the oxide scales at the bond coat grain boundary protrusions. Total number of thermal cycles affect the density of microcracks within the TGO layer. Evidence is presented that higher density of microcracks in the 10-min hold-time experiments tend to separate the TBC from the TGO layer via extensive coating "micro-decohesion" and promotes 'complete' TBC separation as opposed to traditional 'partial' spallation of TBC from the substrate as in the 45-min hold-time and isothermal experiments.

1. Introduction

Thermally grown oxide layer (TGO) forms between TBC/bond coat interface in a TBC-superalloy system when exposed to high temperature. The TGO layer forms when depleted aluminum from bond coat reacts with the oxygen that seeped through YSZ TBC. In the literature, researchers presented numerous damage/spallation models for the TBC-Superalloy system based on the detrimental effects of this TGO [1–5].

Nusier *et al*. [6] investigated the effect of different thermal cycles on TBC spallation lifetime. They associated a critical oxide thickness (12 μm) with spallation life for the 8 wt% YSZ/PtAl/Rene N5 EB-PVD system. They also showed that spallation lifetime increased significantly with decreasing maximum exposing temperature.

Evans *et al*. [7] investigated the effect of interface undulation on the thermal fatigue of thin films and scales on metal substrate. They proposed that interface nonplanarity can result in cyclic straining of the substrate, near the interface, leading to crack initiation by fatigue.

While developing a spallation model for a TBC-Superalloy system, many researchers assumed the presence of an initial interface separation. Upon cooling, a compressive stress develops in the TBC due to thermal expansion mismatch between the layers and it is suggested that it causes the buckling of TBC and leads to spallation [1–5] or an oxidation-based model where TGO growth to a certain thickness causes spallation [8, 9]. Since the development of an initial separation constitutes an important prerequisite for the spalling process, an understanding of its development needs further clarification. The present work further attempts to explain the cause of spallation of TBC from substrate by reviewing the mechanisms for void growth (inception of microcracks) and other relevant findings from literature. Also, this work utilizes the damage growth concept to explain why different hold times and cycling conditions result in different lifetimes for TBC spallation as found from the experiments.

2. Experimental procedures

The TBC-superalloy samples (8 wt% YSZ/PtAl/Rene N5) used for the present work were prepared by General Electric Aircraft Engines. Electron Beam Physical Vapor Diposition (EB-PVD), a thermal evaporation process conducted under high vacuum, was used to apply the ZrO_2-Y_2O_3 coatings. The target material (ZrO_2-Y_2O_3) is usually heated above its evaporation temperature ($T \geq 3500$ °C) by a high power electron beam, and the resulting vapors were condensed onto a rotating substrate of bond coated Rene N5, which was maintained at a temperature of 1000–1050 °C during deposition [7, 10, 11]. To maintain stoichiometry of the ceramic coating, some oxygen was bled into the chamber during deposition. Because of this, a submicron layer Al_2O_3 forms due to oxidation on the bond coat adjacent to the

* Author to whom all correspondence should be addressed.

TABLE I

Cycle Type	Min. Temp. °C (T_{min})	Max. Temp. °C (T_{min})	Heating Time (min) t_1	Holding Time (min) t_2	Cooling Time (min) t_3	Sample Tested	Spall off Cycles/Hrs
A	200	1177	9	45	10	4	175-180 cyc.
B	500	1177	5	10	2	6	525-600 cyc.
C	—	1177		Isothermal		3	150-180 hrs.

thick (127 μm) ceramic coating [10, 12]. Pt-Al bond coat also deposited on the substrate at a temperature ∼1000 °C [13]. When the TBC-superalloy system was exposed to high temperature during experiment, bond coat is further oxidized and results in a thicker TGO layer formed between the bond coat and the TBC.

The specimen used is a small disk having a diameter of 25.4 mm (superalloy substrate René N5 of thickness 3.175 mm). It is overlayed with diffusion aluminide Pt-Al alloy bond coat (thickness 0.36 mm) and 8 wt.% yttria stabilized zirconia (YSZ) TBC (thickness 0.127 mm). This specimen is named as type 1 for reference. The type 2 specimen is the same as type 1 except that there is no TBC layer. The purpose of using this specimen is to investigate the failure of TGO layer and associated microstructural features developed during different types of thermal cycling.

A number of type I and type II specimens were placed in a muffle-type rapid heating/cooling furnace and thermally cycled. The specimens were tested for thermal cycles of type A, B and C (these are typical standards used by GE to select materials). The thermal cycle profiles used to run these tests are shown in Table I and Fig. 1. For type A thermal cycle the holding time was 45 minutes at the peak temperature (1177 °C) in each cycle. The heating time was 9 minutes to reach the peak temperature and the cooling time was 10 minutes to reach the lower temperature of the cycle. For type B thermal cycle, the peak temperature (1177 °C) holding time was 10 minutes, heating time to reach the peak temperature was 5 minutes and cooling time was 2 minutes to reach the lower temperature of the cycle. A muffle-type rapid heating/cooling furnace was used for type A and B thermal cycles. A CARBOLITE RHF 1400 furnace was used for type C isothermal condition. Scanning electron microscopy was carried out by using a Hitachi 2000 SEM on type I (after TBC spalled) and type II specimens to investigate the growth of microcracks in TGO.

3. Results and discussion

3.1. Oxide scale development

Based on the processing temperatures involved in the coating process (YSZ, Pt-Al), it has been assumed that the processing temperature to be precisely 1000 °C. The PVD TBC relies on a chemical bond between a smooth bond coat and the alumina scale that forms on the bond coat and the YSZ [12, 14]. So it is assumed that the four layers - TBC, bond coat, TGO and substrate, respectively, are stress free at the layer interfaces at the processing temperature (1000 °C). Thus, temperature variation from the processing temperature causes the thermal expansion mismatch between the respective layers. Since each layer which is bonded with the adjacent layers by chemical bonding, so it is likely that stress reversal (due to temperature reversal corresponding to the processing temperature) may damage an interface if defects are present.

The experimental curves of thermal cycling are shown in Fig. 1b and c. The curves show that the slope of the heating curve decreases considerably when reaching the maximum holding temperature. Thus at ∼1000 °C the specimen was exposed for 50 sec. (Type B cycle, Table I) and for 80 sec. (Type A cycle, Table I) for oxidation. Therefore, it was assumed for simplicity that there are two types of oxides (Al_2O_3); the first type is category 1 that formed in the vicinity of 1000 °C along with the oxide layer during processing and the second type is category 2 that formed at highest temperature (1177 °C, for the present case). The category 2 oxides that formed at 1177°C is assumed to be thermal stress free at that holding temperature and will not see any creep effect [15]. However, those oxides that formed at ∼1000 °C will experience a tensile stress and will creep to the zero stress at the holding time (if exposed for sufficient time) [15]. Then both types of TGO will be in zero-stress state and upon cooling will exhibit the same large compressive stress in the TGO layer. Under creep conditions, polycrystalline solids often rupture prematurely by the growth and coalescence of grain boundary microcracks. These microcracks originate from grain boundary voids [16]. Concentrated void population generally forms on grain boundaries oriented in a direction perpendicular to the applied tensile load [17]. For the alumina scale that formed at the processing temperature, microcracks may have formed at the grain boundaries due to tensile stress (material flows and is highly ductile at high temperatures) when heated above the processing temperature and due to compressive stress while cooled down far below the processing temperature. Type A thermal cycle was likely to cause TGO to fail in that way via growth of microcracks randomly, primarily due to cool-down residual stresses.

If category 1 oxide layer doesn't get enough time to creep to zero stress then upon cooling there will be stress difference in the oxide layer itself. It should be noted here that at the holding temperature 1177 °C, the tensile stress on the oxide that formed at ∼1000 °C is large enough to lead to microcracking/failure at that region [15]. This assumption was based on the alumina properties; tensile strength 150 MPa (at 1200 °C) and compressive strength 3860 MPa (at room temperature) for 100% Al_2O_3. Type B thermal cycle was likely to cause TGO to fail in that way. The idealized schematic

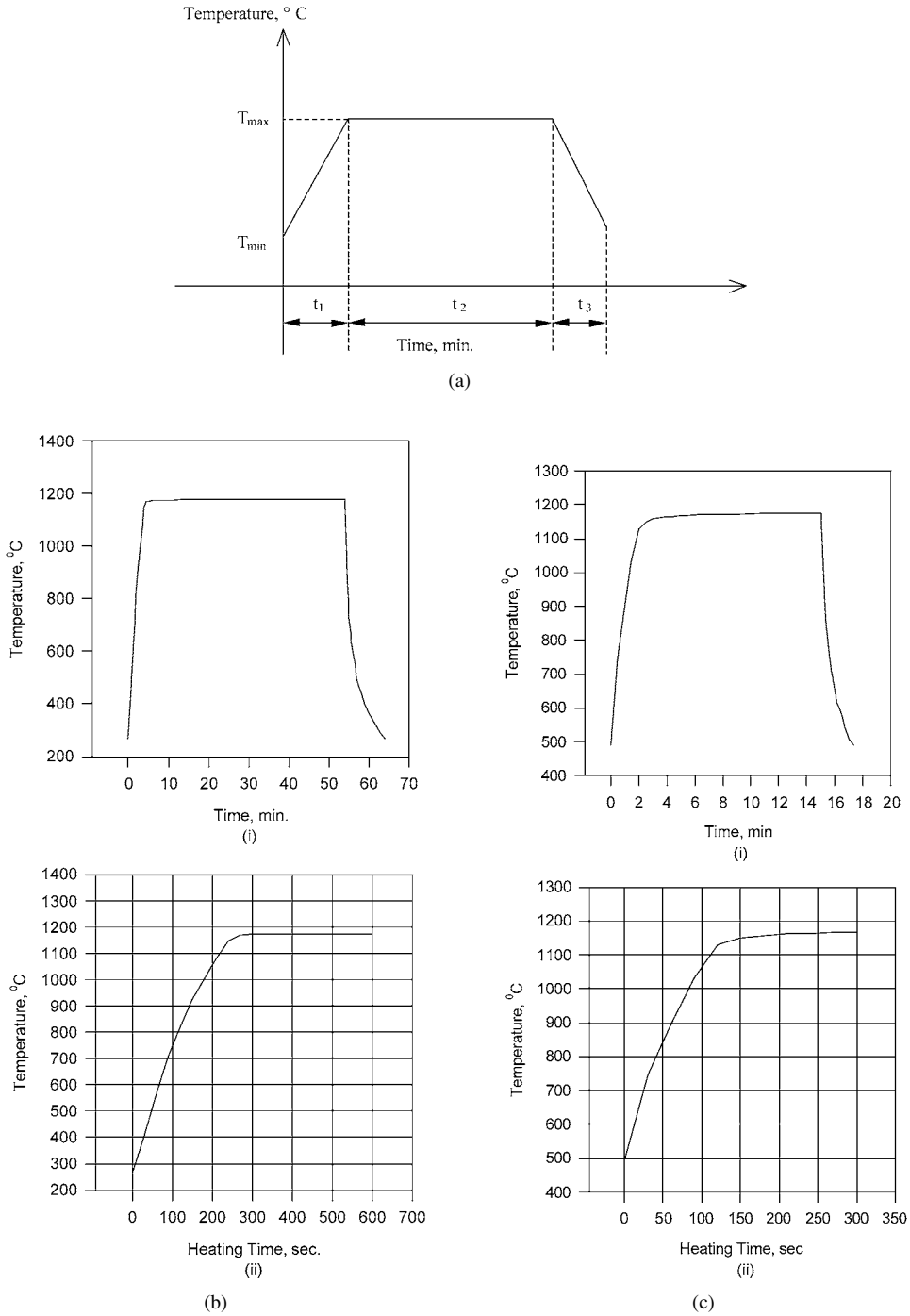

Figure 1 (a) Various thermal cycles used for disk type specimens (Programmed Cycle). (b) (i) Actual Type A thermal cycle profile. (ii) Zoomed view for heating time shows 80 sec elapsed time in the vicinity of ∼1000 °C. (c) (i) Actual Type B thermal cycle profile. (ii) Zoomed view heating time shows 50 sec elapsed time in the vicinity of ∼1000 °C.

view of this oxide layer formation for specimens thermally cycled with type A, B and C (Table I) cycles, is shown in Fig. 2a. From the result of previously reported creep effect on residual stresses in different layers [15], it is obvious that Al_2O_3 layer that formed at ∼1000 °C is more detrimental for the system as it is subjected to both tensile and compressive stresses (Fig. 2b).

Cavities formed at the grain edges create microcracks, which in a favorable condition coalesce together to form large cracks [18]. Both cavities and wedge cracks lead to the totally cracked grain facet as a critical stage in the fracture process. But the continued propagation of microcracks along inclined grain boundaries may take considerable time to develop into macro cracks, which lead to coating spallation/separation and failure.

3.2. Damage evolution in TGO

YSZ TBC is permeable to oxygen [19] and surface topograph of TGO formed at the very beginning of oxidation period remains almost same after long oxidation period [20]. Thus, it is reasonable to visualize the microcrack growth in TGO layer using type 2 specimen to understand the failure nature of type 1 specimen at different cycling. There may be some differences between the growth of TGO adjacent to TBC and on the free surface of bond coat. But this difference can be neglected due to columnar structure of YSZ TBC [14, 21]. The

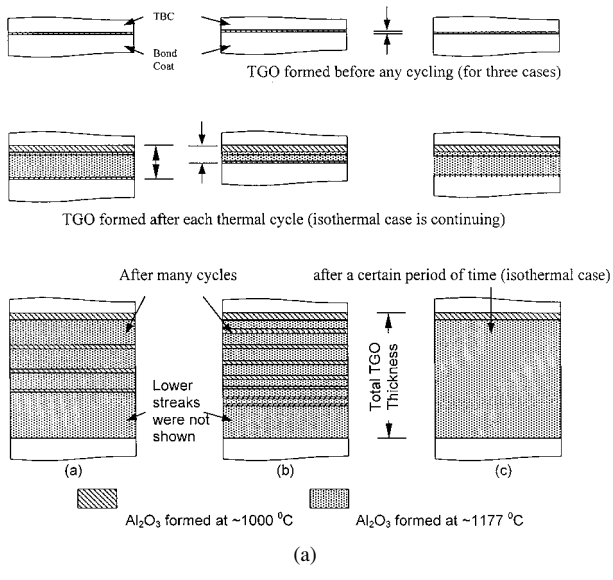

(a)

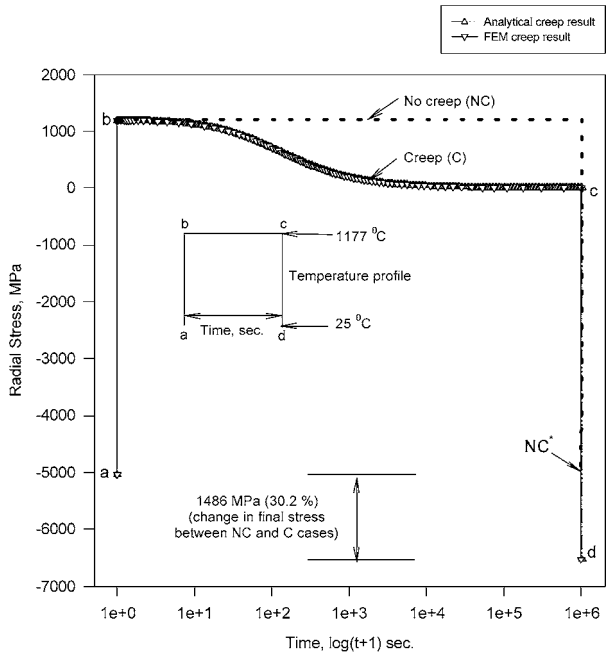

(b)

Figure 2 (a) Idealized schematic (exaggerated) view of (a) TGO formation for type A thermal cycling, streak of Al_2O_3 formed at ~1000 °C is less, (b) TGO formation for type B thermal cycling, streak of Al_2O_3 formed at ~1000 °C is more than type A, (c) TGO formation for type C (isothermal), only one streak of Al_2O_3 formed at ~1000 °C. (b) Thermal loading cycle and corresponding stress vs. time profile in Oxide layer for disk specimen. Analytical and FEM results matches extremely well. NC* represents the final value for NC analysis. [15].

YSZ TBC itself is highly strain tolerant and is expected to provide negligible constraint to the oxide layer. In this work, type 2 specimens were tested for type A and B cycling and their microstructures were investigated by SEM to view microcracks in the oxide layer that can explain the fatigue (cyclic) failure of type 1 specimen. The specimens (type 2) have been viewed in the middle and towards at the end of the cycling period for failure for both type A and B thermal cycles. One specimen of type 1 subjected to two thermal cycle of type A was sectioned and its cross section was viewed by SEM for correlation purpose.

Fig. 3 shows the cross section of a type 1 specimen subjected to two type A thermal cycling. The initiation of damage is obvious and adjacent to the TBC where it is believed that category 1 oxide layer is present. It should be noted that category 1 oxide layer is subjected to both tensile and compressive stress. Guiu [22] compared the fatigue behavior of alumina under tension-compression cycling and static loading by using tension specimens without artificial cracks. He showed that cracks propagate faster under tension-compression cycling than under static loading. Kim and Suh [23] investigated the effect of compressive stress on the fatigue behavior of alumina by comparing experimental data under uniaxial (i) tension-unloading and (ii) tension-compression cycling. They found that under tension-compression cycling, residual tensile strains developed. However, under tension-unloading, the residual tensile strains were not observed. Brockenbrough and Suresh [24], showed that large residual tensile stresses are induced in the vicinity of the notch when micro cracks were blocked from closure due to crack surface friction or debris at unloading from compression. Thus, residual tensile strains in tension-compression cycling may be caused by this microcracking mechanism. Reece *et al.* [25], reported that far-field compressive loads produce a bending moment around the wedging or sliding asperities at the crack surface. They also explained that the bending moment may enhance both the tensile and shear stresses at the crack tip.

Fig. 4 shows the top surface of a untested type 2 specimen. Fig. 5 shows the top surface of type 2 specimen after 75 A-type cycles. Some bond coat grains along with TGO are pushed a little bit upward (dislocated) because of "push-pull" action. These bond coat grain boundary protrusions are initiation

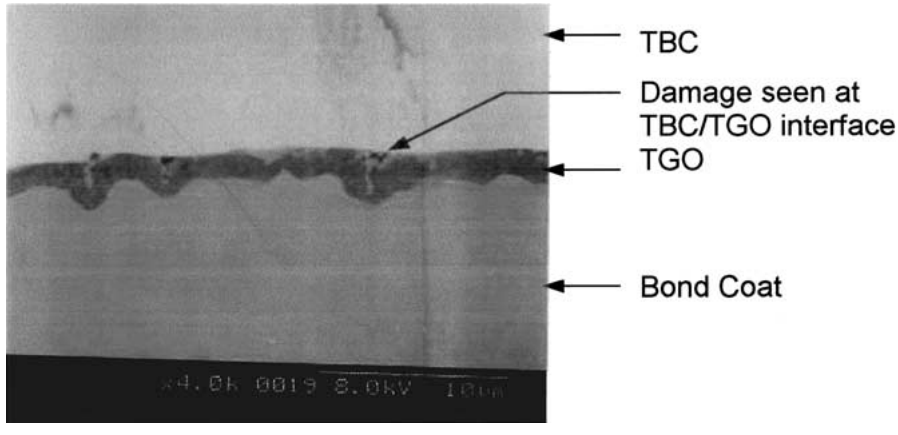

Figure 3 Section cut of type 1 specimen subjected to two type A thermal cycles.

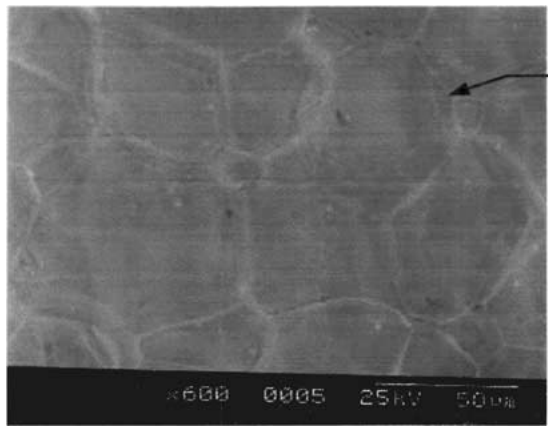

Figure 4 Top surface (bond coat) of untested type 2 specimen.

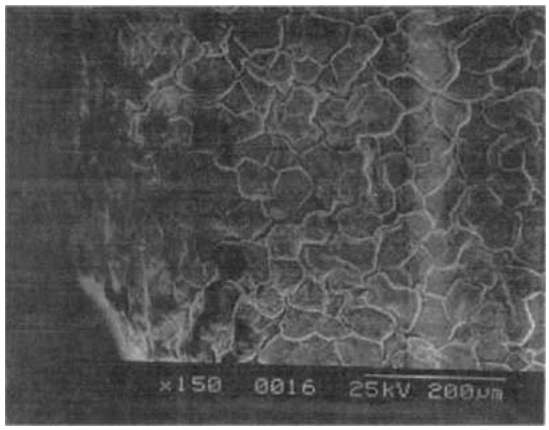

Figure 5 The top surface of type 2 specimen after 75 A cycles. Some bond coat grains are pushed a little bit upward.

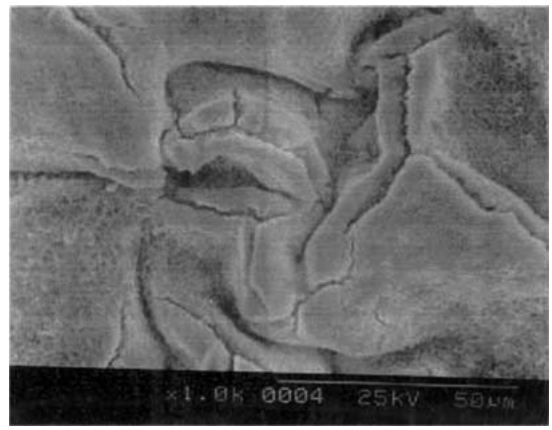

Figure 7 The top surface of type 2 specimen after 150 A cycles. More cracks seen than that of 75 A cycles.

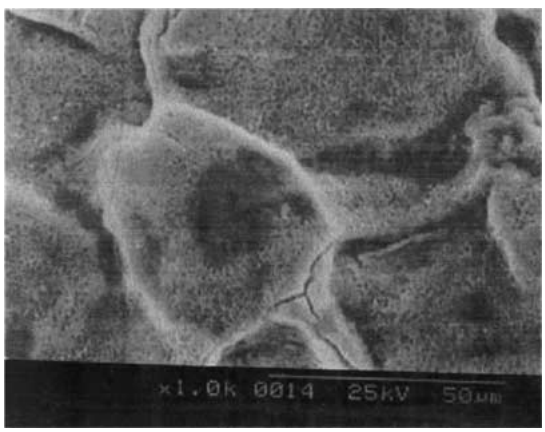

Figure 6 The top surface of type 2 specimen after 75 A cycles. Some cracks are at the impression of bond coat grain boundary.

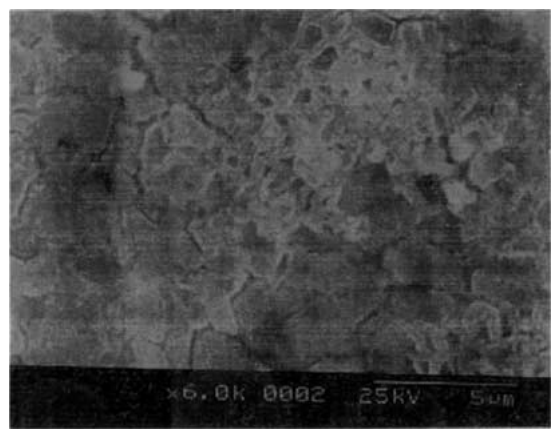

Figure 8 The top surface of type 2 specimen after 175 A cycles. Separation of oxide grains is seen but crack density is relatively small compared to 550 B cycles (Fig. 10(b).

sites for the oxide scale microcraks. Figs 6 and 7 show the cracks grown in the oxide layer of type 2 specimen after type A thermal cycle. Large cracks are at the impressions of bond coat grain boundary. Fig. 8 shows the microcrack development in the oxide grain boundaries of the same specimen (at 175 cycles). Figs 9 and 10 show the crack growth nature for type 2 specimen subjected to type B cycle. Here large cracks at the impressions of bond coat grain boundary were not like those shown in Figs 6 and 7. This was because of the higher stress difference between the higher and lower temperatures. Larger stress difference resulted in larger compressive stress (for same high temperature), which leads to failure at undulations [6, 7]. In this case (type B cycling) more oxide grain boundary separation is observed (Fig. 10b). This is likely because more cycles cause more fatigue and resulted in more grain boundary separation i.e. microcracks. Fig. 11 shows the evidence of both wedging and sliding asperity inside a crack in TGO, which with further cycling will help to grow this

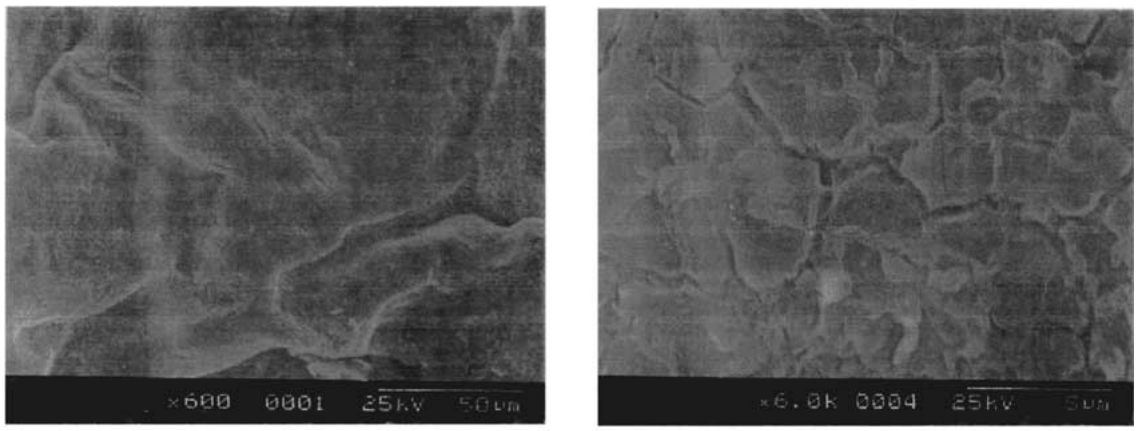

Figure 9 The top surface of type 2 specimen after 337 B cycles. (a) Large cracks are not seen like found in 75 A cycles. But (b) the oxide grain boundary separation is seen.

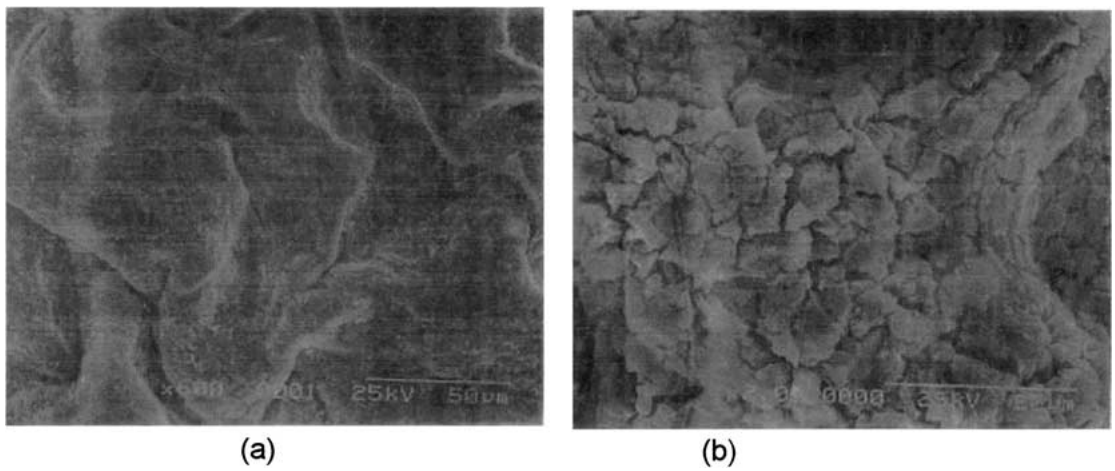

Figure 10 The top surface of type 2 specimen after 550 B cycles. (a) Large cracks are still not seen like found in 150 A cycles. But the oxide grain boundary separation (b) is found almost all over the TGO surface.

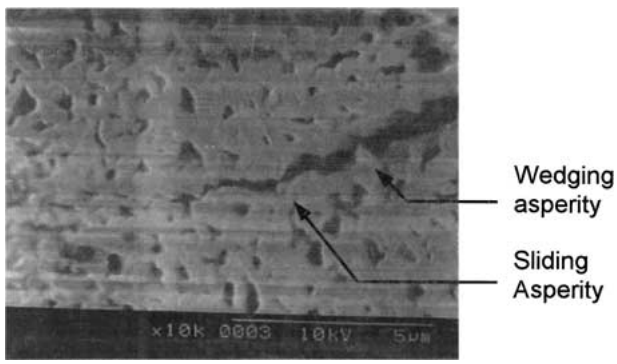

Figure 11 The top surface of type 2 specimen after 100 A cycles. The picture is showing the evidence of both wedging and sliding asperity on the cracked surfaces.

crack. When this specimen was raised to maximum holding temperature, oxide formed on the cracked face and upon cooling these wedges and sliding asperities likely caused the compressive stress on the far side of crack tip to develop a tensile stress at the crack tip. The crack grew, when the stress limit exceeded the material strength limit. Because of "pull-push" action in type A and B thermal cycling, the oxide grains are forced to separate with time. So, it is likely that TBC will spall prematurely and debond if enough oxide grains of the TBC/oxide interface are separated.

3.3. Spallation in TBC system

Figs 12 and 13 show the failure nature of type 1 specimen when subjected to thermal cycle of type A and C, respectively. The failure nature is different from that of Fig. 14a and b that shows the failure of type 1 specimen subjected to type B thermal cycling. This is likely due to the fact that in type B thermal cycling, more layers of category 1 oxide forms (conceptually) than that due to type A (Fig. 2a). In this case, more cracks must be present in the oxide layer of type B thermal cycling than that for type A. Also, more cracks enhance the oxidation rate and more debris are likely to appear in the crack face. The type B thermal cycling is more severe than type A because the number of layers of category 1 oxide is higher and these layers are likely to carry more defect populations which may cause more void growth and cracks in grain boundaries. Since type B thermal cycling is more favorable for grain separation, thus cracks distribute more evenly in the oxide layer than type A. Also, because of smaller hold time, the distance between two category 1 oxide layers is smaller than that for type A cycling. That helps the

Figure 12 The spallation nature of type 1 specimen after 180 type A thermal cycles.

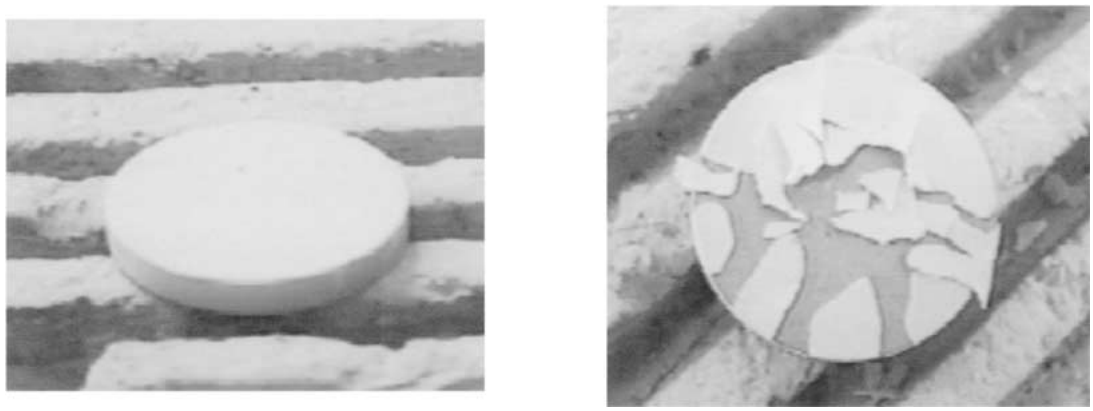

Figure 13 The spallation nature of type 1 specimen after 180 hrs of isothermal (type C thermal cycle) testing.

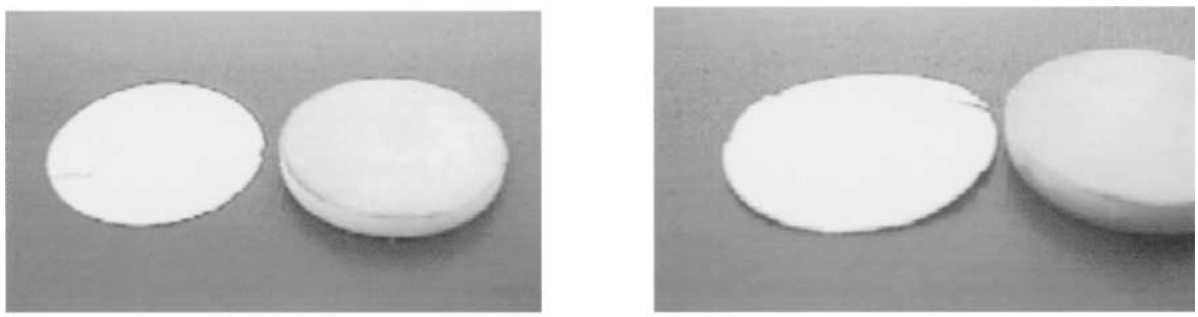

Figure 14 The spallation nature of type 1 specimen after (a) 525 cycles and (b) 600 cycles of type B thermal cycle. With 550 and 575 type B thermal cycles same spallation nature has been seen.

microcrack coalescence in interlayer for type B thermal cycling. Thus, upon cooling after a particular number of type B thermal cycling, a comparatively small buckling stress may cause the whole TBC layer to separate from oxide layer. Essentially, an extensive micro-decohesion of TBC from the bond coat can be anticipated due to microcracks in the TGO layer.

It should be noted that the oxide/bond coat interface degradation occurs with time [26]. Therefore, for type A and B thermal cycling, failures due to cracks are more likely than degradation failure. For type C, the failure is completely by oxide/bond coat interface degradation [26]. From investigation it was found that for type B thermal cycling the surface of failed TGO showed a very clear view that cracks grew step-by-step, and more debris inside the cracks. For isothermal case, the oxide layer after TBC spalled showed a very sharp surface feature and no trace of TGO grain separation. This indicates that the TBC spalled at once and there is no sign of step-by-step microcrack growth.

From experiment, it is found that high temperature exposure period (HTEP) is smaller for type B cycling (525–600 cycles, HTEP is 5250–6000 min.) than Type A (175–180 cycles, HTEP 7875–8100 min.) and C (150–180 hrs., HTEP 9000–10800 min.). One would anticipate that the TGO layer for 10 min cycling sample (Type B) will not be as thick compared to Type A and Type C cycling samples. Since failure is occurring in

less time in terms of HTEP (with less oxide thickness) it implies that cycling has a major effect in lowering life. It is anticipated that cycling will promote additional damage (microcracks) within the TGO layer.

4. Conclusions

A methodical approach was used to investigate the role of TGO layer breakdown on the spallation mechanisms for various types of thermal cycling conditions. This involved experiments with and without TBC. For thermal cycling conditions, the breakdown of the TGO layer was found to be due to extensive microcracking which manifests either as 'partial' or 'complete' decohesion of the TBC layer from the bond coat.

The microcrack density in the TGO layer for higher number of short-duration (10 min.) thermal cycles is higher compared with long duration (45 min.) thermal cycles and isothermal conditions. Therefore, higher number of short duration thermal cycles result in extensive decohesion of TBC layer from the TGO, which promotes complete separation. For the longer-duration thermal cycling and isothermal conditions, decohesion is partial which result in local spallation of TBC from TGO.

A conceptual model (Fig. 2a) is forwarded for the growth of the TGO layer for various cycling and isothermal conditions. Microcracking density and their interaction in the evolving TGO layers due to the thermal cycling conditions can be rationalized using the conceptual model to address why a 'partial' or a 'complete' separation of the TBC would be preferred. The investigation also points out that the spallation process can be viewed as a "micro-decohesion" process influenced by both oxidation and physical microcracking process of the TGO layer due to residual stresses and possibly their reversal during thermal excursion.

Acknowledgment

Funding for this research was provided through a grant (#F49620-98-1-0390) from the Air Force Office of Scientific Research (AFOSR). Dr. Thomas Hahn was the program monitor. Discussion and interaction with Dr. P. K. Wright of GEAE is gratefully acknowledged.

References

1. A. G. EVANS, G. B. CRUMLEY and R. E. DEMARAY, *Oxidation of Metals* **20**(5/6) (1983) 193.
2. H. E. EVANS, *Materials at High Temperatures* **12**(2-3) (1994) 219.
3. *Idem., Materials Science and Engineering* **A 120** (1989) 139.
4. Z. H. JIN and R. C. BATRA, *Int. J. Engng. Sci.* **34**(15) (1996) 1705.
5. Z. SUO, Report, University of California, Santa Barbara, 1994.
6. G. M. NEWAZ, S. Q. NUSIER and Z. A. CHAUDHURY, *Engineering Materials and Technology* **128**(2) (1998) 149.
7. A. G. EVANS, M. Y. HE and J. W. HUTCHINSON, *Acta Mater.* **45**(9) (1997) 3543.
8. K. S. CHAN, *Metallurgical and Materials Transactions A* **28A** (1997) 411.
9. R. A. MILLER, *J. Amer. Ceram. Soc.* **67**(8) (1984) 517.
10. O. UNAL, T. E. MITCHELL and A. H. HEUER, *ibid.* **77**(4) (1994) 984.
11. U. SCHULZ, K. FRITSCHER, C. LEYENS, M. PETERS and W. A. KAYSSER, *JOM* **49**(10) (1997).
12. D. V. RIGNEY, R. VIGUIE and D. J. WORTMAN, Proceedings of Conference, March 27–29, NASA Lewis Research Center, Ohio (1995) p. 135.
13. R. STREIFF and D. H. BOONE, "Coatings and Bimetalics for Aggressive Environments," Conference Proceedings of ASM (1985) p. 159.
14. A. MARICOCCHI, A. BARTZ and D. WORTMAN, Proceedings of Conference, March 27–29, NASA Lewis Research Center, Ohio (1995) p. 79.
15. M. Y. ALI, MS thesis, Department of Mechanical Engineering, Wayne State University, Detroit, MI, 1999.
16. R. RAJ and M. F. ASHBY, *Acta Metallurgica* **23** (1975) 653.
17. T. CHUANG, K. I. KAGAWA, J. R. RICE and L. B. SILLS, *ibid.* **27** (1979) 265.
18. H. E. EVANS, "Mechanics of Creep Fracture" (Elsevier Applied Science Publication Ltd., London, 1984).
19. F. O. SOECHTING, Proceedings of Conference, March 27–29, NASA Lewis Research Center, Ohio (1995) p. 1.
20. E. J. FELTON and F. S. PETTIT, *Oxidation of Metals* **10**(3) (1976) 189.
21. R. A. MILLER, Proceedings of Conference, March 27–29, NASA Lewis Research Center, Ohio (1995) p. 17.
22. F. GUIU, *J. Mater. Sci. Lett.* **13** (1978) 1357.
23. K. T. KIM and J. SUH, *J. Amer. Ceram. Soc.* **76**(1) (1993) 229.
24. J. R. BROCKENBROUGH and S. SURESH, *J. Mech. Phys. Solids* **35** (1987) 721.
25. M. J. REECE, F. GUIU and M. F. R. SAMMUR, *J. Amer. Ceram. Soc.* **72** (1089) C-348.
26. Y. H. SOHN, R. R. BIEDERMAN and R. D. SISSON, JR., *J. Materials Engineering Performance* **3** (1994) 55.
27. S. Q. NUSIER, Ph.D. Dissertation, Wayne State University, Detroit, MI, 1997.
28. H. C. CHANG and N. G. GRANT, *Trans. Am. Inst. Min. Metall. Eng.* **204** (1956) 544.

Received 8 February 2000
and accepted 16 January 2001